

**Estimating the Time Course of Pore Expansion
during the Spike Phase of Exocytotic Release in
Mast Cells of the Beige Mouse**

Brenda Farrell¹ and Steven J. Cox²

1 Department of Biochemistry and Cell Biology and Keck Center for Computational Biology and

2 Department of Computational & Applied Math., Rice University, 6100 S. Main, Houston, TX 77005.

Corresponding Author: Brenda Farrell,
email: bfarrell@bmc.tmc.edu

Key phrases

fusion pore, diffusion, dynamic Robin condition, inverse problem

Abstract

Our objective is to determine the time course of exocytotic fusion pore opening (P) in mast cells of the beige mouse from the measured efflux of the spike phase of exocytotic release (J). We show that a pore whose meridian or radius grows linearly with time cannot reproduce the efflux. We also show that a pore that opens very quickly (relative to the diffusivity of 5-hydroxytryptamine (5-HT)) and completely ($P = \pi$) also does not mimic the experimental efflux, and estimate maximum pore angles between 45 and 100° . We show that a larger class of opening functions reproduces the rising phase and part of the decay phase and calculate pore expansion rate; pore radius and pore angle, none of which can be readily measured. In the initial stages of the spike phase (50-200ms) when the gel matrix has not expanded significantly we found that pore radius increases exponentially with a time constant of $82 (\pm 62)$ ms with pore expansion reaching its maximum velocity of $20 (\pm 7)$ nmms⁻¹. We conclude that the release process is dynamic and suggest that the velocity of pore opening (V) and the diffusivity of 5-HT (D), in addition to the size of the vesicle (R , radius) vary with time. We discuss assumptions and improvements to the model and propose that this methodology is applicable for determining P from measured J in other endocrine cells and neurons when D within the secretory vesicle is much less than D within the pore neck.

1. Introduction

Exocytotic release of small secretory products from mast cells is controlled by both the diffusivity of participating molecules and pore geometry. Freeze fracture images from mast cells undergoing exocytosis reveal that the fusion pore is hourglass shaped (Chandler and Heuser 1980 and Curran *et al.* 1993). Evidence suggests that small charged secretory molecules such as serotonin and histamine diffuse from the vesicle through the exocytotic fusion pore by ion-exchange (Uvnas and Aborg 1977). This is surmised from a body of information which includes: charged products are condensed by a highly negatively charged matrix within the lumen of the vesicle (Yurt *et al.* 1976 and Uvnas *et al.* 1985); the interaction between heparin a major component of the matrix and histamine is electrostatic and strongly dependent upon the sodium ion concentration (Rabenstein *et al.* 1998); and the effective diffusivity of serotonin within the secretory granule of mast cells of the beige mouse is close to a typical ion exchanger (Marszalek *et al.* 1997b).

Admittance measurements of exocytosis in mast cells reveal that initial pore size is small and then slowly expands at a rate of 100 to 200 pSms⁻¹; pore size then fluctuates around a mean value and expands irreversibly or it retracts and the pore closes (Spruce *et al.* 1990, Nanavati *et al.* 1992 and Curran *et al.* 1993). The dynamics of pore expansion were correlated with the release of biogenic amines in mast cells (Alvarez de Toledo *et al.* 1993) and chromaffin cells (Albillos *et al.* 1997) when release was measured by amperometry with a carbon fiber electrode. In both cases a transient oxidation current or “foot” is observed when the exocytotic fusion pore is small ($< 20nS$), and a large spike-like current follows the foot signal when the conductance becomes immeasurably large. The fusion pore was also observed to flicker and then close as deduced from simultaneously diminishing foot and admittance signals. A single spike without foot signal was also observed with minimal delay after fusion (Alvarez de Toledo *et al.* 1993). Foot and spike signals were detected during release from other endocrine cells (Zhou and Misler 1995a, Urena *et al.* 1994) and during exocytotic release from large dense core vesicles in several neurons (Bruns *et al.* 2000, Bruns and Jahn 1995, Zhou and Misler 1995b). All evidence suggests that a foot represents release through a small metastable fusion pore while a “spike” usually represents release through a pore that expands irreversibly. Possible origins for the spike shape were described in (Schroeder *et al.* 1996). Recently, Amatore *et al.* (1999, 2000) show that the expansion of the pore can be numerically extracted from the spike phase obtained from chromaffin cells undergoing exocytotic release. They do this by assuming that the matrix swells and the fusion pore expands completely and rapidly, relative to the time it takes molecules to diffuse from the lumen of the granule.

Recent theoretical studies of model fusion pores show that pore expansion is driven by the sum of tension in both fusing membranes and predicts that pore radius should increase exponentially during final pore widening (Chizmadzhev *et al.* 2000). In this communication we also show that it is possible to estimate pore characteristics from the spike phase of release for mast cells of the beige mouse, and we present evidence that pore radius does indeed increase exponentially. In §2 we formulate the problem of exocytotic release as diffusion from a sphere subject to a dynamic boundary condition and offer a precise statement of the inverse problem; recover the opening function from the measured efflux. In §3 we prove that the efflux indeed uniquely determines a smooth opening function. In

§§4 and 5 we restrict ourselves to narrow, though natural, classes of opening functions. More precisely, we document the extent to which pores, whose meridian or radius grows linearly with time or that open fast and fully (*a la* Amatore *et al.* 1999, 2000), fail to reproduce the efflux measured from mast cells of the beige mouse. We therefore turn in §6 to a least squares procedure over a wide class of potential opening functions. In the closing sections we outline the limitations of our methods and argue that this general approach leads to similar conclusions to those derived by energetics (Chizmadzhev *et al.* 2000). We suggest that this analysis is of general validity and particularly relevant when assessing the role of fusion proteins on the dynamics of pore expansion (Graham and Burgoyne 2000 and Fisher *et al.* 2001).

2. Diffusion Subject to a Dynamic Boundary Condition

We use patch-clamp amperometry to measure membrane fusion and release (Alvarez de Toledo *et al.* 1993) from mast cells of the beige mouse, see Appendix 1 for experimental methods. Typical recordings that exhibited minimal delay after fusion (< 100 ms) are shown in Figure 1. We focus on the spike phase of release and only show events that exhibit no pre-spike features (i.e. foot phase, Figure 1B). The spike typically exhibits a non-instantaneous rising phase and a decay phase. We also show the time course of the integral; at small times it is typically convex and reaches a plateau at longer times, Figure 1C. Similar to that observed for isolated granules (Marszalek *et al.* 1997a and b) we observe a relationship between the radius of the vesicle and the time of release as assessed by the three time parameters t_{\max} : the time to reach maximum efflux, $t_{1/2}^{\text{int}}$: the time at which 1/2 of the molecules are released and $t_{1/2}^{\text{spike}}$; the width of the spike at half-maximum (Figure 2). Our objective is to explain such relationships and determine the time course of pore opening from such spikes.

During *in vivo* anaphylactic stimulation of mast cells, the secretory granule remnants or gel matrix is observed to adhere onto the outside of the cell (Nielsen *et al.* 1981). This evidence indicates that the pore can get sufficiently large to expel or degranulate the matrix from vesicles. Similar results were observed *in vitro* with beige mast cells, where electron microscopy images illustrate degranulation of some vesicles (Dvorak *et al.* 1987). Similarly, freeze fracture images of rat mast cells illustrate that pore diameter can vary from a size of 22 nm to a very large size of 1300 nm (Curran *et al.* 1993). We are interested in describing release during the final stage of pore widening when the radius of the pore can become comparable to the radius of the fusing vesicle. So unlike studies where the pore is considered small relative to the size of the fusing objects (Nanavati *et al.* 1992 and Chizmadzhev *et al.* 1995 and 2000), we consider vesicle size and define a pore by an angle that subtends a spherical vesicle of radius, R (Figure 3B). Although the pore has length (Figure 3A) we omit pore length at this stage because the length cannot be determined from experiments. Likewise we do not consider broadening of the signal from the vesicle to the fiber because this distance also cannot be determined from experiments. The plots in Figure 4B and C show that it is reasonable to exclude the time taken to diffuse through the neck from the model, when the diffusivity through the vesicle is much less than that through the neck. This is the case for mast cells of the beige mouse where

the effective diffusivity for serotonin within the vesicle was found to be 300 times less than that in the bulk at $2 \times 10^{-8} \text{ cm}^2\text{s}^{-1}$, when determined from isolated granules from the mast cell of the beige mouse, and 30 times less than the bulk at $2.9 \times 10^{-7} \text{ cm}^2\text{s}^{-1}$, when determined from the foot phase of exocytotic release (Marszalek *et al.* 1997b). This is a poor approximation when the diffusivity of transmitter has a similar value in both the vesicle and neck, in this case the time for the molecules to diffuse through the neck may be rate determining, as shown in Figure 4A. Note, we do not model release as an ion-exchange process *per se*, but examine it by employing an effective diffusion constant, D that reflects the slower diffusivity of amines within an ion-exchanger (Marszalek *et al.* 1997b).

We denote by $C(r, \phi, \theta, t)$ the concentration of biogenic amines at the point (r, ϕ, θ) at time t . We suppose at the onset of fusion, $t = 0$, that the concentration of neurotransmitters is uniform throughout the vesicle, i.e.,

$$C(r, \phi, \theta, 0) = C_0, \quad 0 \leq r < R, \quad 0 \leq \phi < 2\pi, \quad 0 \leq \theta < \pi, \quad (2.1)$$

where C_0 is constant. The concentration at all future times is governed by the diffusion equation (Crank 1976, eqn. (1.8))

$$C_t = D \left\{ \frac{1}{r^2} (r^2 C_r)_r + \frac{1}{r^2 \sin \theta} (C_\theta \sin \theta)_\theta + \frac{1}{r^2 \sin^2 \theta} C_{\phi\phi} \right\}, \quad (2.2)$$

with a fixed diffusivity, D , together with boundary conditions that reflect the opening of a pore. To be precise, we equate the pore at time t with the spherical cap (Figure 3B, inset)

$$\{(R, \phi, \theta) : 0 \leq \phi < 2\pi, \quad 0 \leq \theta \leq P(t)\} \quad (2.3)$$

where P is the ‘opening function’ of the pore. If each molecule reaching the pore is absorbed and no molecules cross the intact boundary of the vesicle then C obeys the boundary conditions

$$\begin{aligned} C(R, \phi, \theta, t) &= 0 \quad \text{when } \theta < P(t), \\ C_r(R, \phi, \theta, t) &= 0 \quad \text{when } \theta > P(t). \end{aligned} \quad (2.4)$$

We denote the point-wise flux by

$$j(\phi, \theta, t) = -DC_r(R, \phi, \theta, t)$$

and its integral over the vesicle’s boundary by

$$J(t) = R^2 \int_0^{2\pi} \int_0^\pi j(\phi, \theta, t) \sin \theta \, d\theta d\phi.$$

As the initial and boundary data are independent of ϕ , so too is the concentration, C , and hence (2.2) becomes

$$(r^2 \sin \theta) C_t = D((r^2 \sin \theta) C_r)_r + D((\sin \theta) C_\theta)_\theta. \quad (2.5)$$

It is convenient to work with the nondimensional variables

$$\rho \equiv \frac{r}{R}, \quad \tau \equiv \frac{Dt}{R^2}, \quad c(\rho, \theta, \tau) \equiv \frac{C(r, \theta, t)}{C_0}, \quad \text{and} \quad p(\tau) \equiv P(t). \quad (2.6)$$

In subsequent sections we consider pores that open at constant velocity, V . Its nondimensional counterpart is

$$v \equiv \frac{VR}{2D}. \quad (2.7)$$

The diffusion equation, (2.5), becomes, in these variables

$$(\rho^2 \sin \theta) c_\tau = ((\rho^2 \sin \theta) c_\rho)_\rho + (c_\theta \sin \theta)_\theta, \quad (2.8)$$

while the initial and boundary conditions become

$$c(\rho, \theta, 0) = 1, \quad (2.9)$$

and

$$\begin{aligned} c(1, \theta, \tau) &= 0 & \text{when } \theta < p(\tau) \\ c_\rho(1, \theta, \tau) &= 0 & \text{when } \theta > p(\tau). \end{aligned} \quad (2.10)$$

The piecewise nature of (2.10) is an idealization of the actual set up and, though simple to state, complicates our analysis and numerics. In reality the pore is not perfectly absorbing and so we posit a nondimensional pore resistance, ε , in which case (2.10) becomes

$$H(p(\tau) - \theta) c(1, \theta, \tau) + \varepsilon c_\rho(1, \theta, \tau) = 0, \quad 0 \leq \theta < \pi \quad (2.11)$$

where H is the Heaviside function

$$H(x) = \begin{cases} 0 & \text{if } x \leq 0 \\ 1 & \text{if } x > 0. \end{cases}$$

Though p now appears as a coefficient in the boundary condition it falls in the argument of a discontinuous function. We therefore approximate H with the sigmoidal

$$H_\delta(x) = 1 + \frac{2}{\pi} \arctan \left(\frac{x}{\delta} \right)$$

for small δ and arrive at the dynamic Robin condition

$$\varepsilon c_\rho(1, \theta, \tau) + H_\delta(p(\tau) - \theta) c(1, \theta, \tau) = 0, \quad 0 \leq \theta < \pi. \quad (2.12)$$

Finally, the nondimensional efflux takes the form

$$E(\tau) = - \int_0^\pi c_\rho(1, \theta, \tau) \sin \theta d\theta. \quad (2.13)$$

We are interested in the extent to which the measured efflux, J , determines the opening function, p , or, equivalently, the extent to which E determines p . We show in the next section that knowledge of E indeed uniquely determines the smooth opening function, p .

3. The Efflux Uniquely Determines the Opening Function

If p is analytic and c is the solution of (2.8)–(2.9) and (2.12) then it is not difficult to show that c and therefore E are also analytic, (Friedman 1964). We now show that in this case the MacLaurin series of E determines the MacLaurin series of p . Along the way we need to exploit the fact that

$$\partial_\tau^j c(\rho, \theta, 0) = 0, \quad j = 1, 2, 3, \dots \quad (3.1)$$

This may be deduced, for $j = 1$, upon letting $t \rightarrow 0$ in (2.8) and noting that the initial data is constant.

We use (2.12) to write the efflux as

$$\begin{aligned} E(\tau) &= - \int_0^\pi c_\rho(1, \theta, \tau) \sin \theta \, d\theta \\ &= \frac{1}{\varepsilon} \int_0^\pi H_\delta(p(\tau) - \theta) c(1, \theta, \tau) \sin \theta \, d\theta. \end{aligned}$$

We now differentiate with respect to τ and find

$$E'(t) = p'(\tau) \frac{2\delta}{\pi\varepsilon} \int_0^\pi \frac{c(1, \theta, \tau) \sin \theta}{\delta^2 + (p(\tau) - \theta)^2} \, d\theta + \frac{1}{\varepsilon} \int_0^\pi H_\delta(p(\tau) - \theta) c_\tau(1, \theta, \tau) \sin \theta \, d\theta.$$

Letting $t \rightarrow 0$ and recalling (3.1) yields

$$\begin{aligned} E'(0) &= p'(0) \frac{2\delta}{\pi\varepsilon} \int_0^\pi \frac{c(1, \theta, 0) \sin \theta}{\delta^2 + \theta^2} \, d\theta + \frac{1}{\varepsilon} \int_0^\pi H_\delta(-\theta) c_\tau(1, \theta, 0) \sin \theta \, d\theta \\ &= p'(0) \frac{2\delta}{\pi\varepsilon} \int_0^\pi \frac{\sin \theta}{\delta^2 + \theta^2} \, d\theta. \end{aligned}$$

Similarly,

$$\begin{aligned} E''(\tau) &= p''(\tau) \frac{2\delta}{\pi\varepsilon} \int_0^\pi \frac{c(1, \theta, \tau) \sin \theta}{\delta^2 + (p(\tau) - \theta)^2} \, d\theta \\ &\quad + p'(\tau) \frac{2\delta}{\pi\varepsilon} \int_0^\pi \frac{(\delta^2 + (p(\tau) - \theta)^2) c_\tau(1, \theta, \tau) - c(1, \theta, \tau) 2p'(\tau)(p(\tau) - \theta)}{(\delta^2 + (p(\tau) - \theta)^2)^2} \sin \theta \, d\theta \\ &\quad + p'(\tau) \frac{2\delta}{\pi\varepsilon} \int_0^\pi \frac{c_\tau(1, \theta, \tau) \sin \theta}{\delta^2 + (p(\tau) - \theta)^2} \, d\theta + \frac{1}{\varepsilon} \int_0^\pi H_\delta(p(\tau) - \theta) c_{\tau\tau}(1, \theta, \tau) \sin \theta \, d\theta \end{aligned}$$

and so, as $t \rightarrow 0$,

$$E''(0) = p''(0) \frac{2\delta}{\pi\varepsilon} \int_0^\pi \frac{\sin \theta}{\delta^2 + \theta^2} \, d\theta + (p'(0))^2 \frac{2\delta}{\pi\varepsilon} \int_0^\pi \frac{\theta \sin \theta}{(\delta^2 + \theta^2)^2} \, d\theta.$$

The pattern should now be clear. As

$$\int_0^\pi \frac{\sin \theta}{\delta^2 + \theta^2} d\theta \neq 0$$

it follows that, for each j , the value of $d^j p(0)/d\tau^j$ is determined by $d^j E(0)/d\tau^j$ and $d^k p(0)/d\tau^k$ for $k = 0, 1, \dots, j - 1$. Although this procedure is constructive, practical considerations compel us to refrain from developing explicit expressions for each of the derivatives of p . More precisely, as E is sampled at discrete instants we have little confidence in anything beyond its first derivative at 0.

In the next section we attempt to fit the experimental efflux with opening functions drawn from natural classes of one and two parameter families.

4. “Linear” Opening

A number of studies have considered a pore whose radius grows linearly with time, Stiles *et al.* (1996), Khanin *et al.* (1994). We find it useful to also consider a pore whose meridian (surface diameter, Figure 1) grows linearly with time. More precisely, the latter case is described by the opening function

$$P_1(t) = \min(Vt/(2R), \pi) = p_1(\tau) = \min(v\tau, \pi), \quad (4.1)$$

while the former is captured in

$$P_2(t) = \min(\arcsin(Vt/(2R)), \pi/2) = p_2(\tau) = \min(\arcsin(v\tau), \pi/2). \quad (4.2)$$

For pore P_1 molecules diffuse from a curved surface as it unfolds to form a flat sheet (Figure 3C (i) through (v)), while for pore P_2 molecules diffuse from a curved surface that unfolds more quickly, but which then stops unfolding when the pore angle reaches $\pi/2$, (Figure 3C (i) through (iii)).

We use finite element and Monte Carlo methods (Appendix 2) to determine the concentration c subject to either p_1 or p_2 . We calculate c and E for $0.02 \leq v \leq 25$. This range of v for mast cells of the beige mouse is drawn from (2.7) using reported values of D of serotonin ($10^{-8} - 10^{-7} \text{ cm}^2\text{s}^{-1}$ Marszalek *et al.* 1997b), R ($1 - 3 \mu\text{m}$), and V ($0.5 - 25 \text{ nmms}^{-1}$, Spruce *et al.* 1990 and Stiles *et al.* 1996).

Outlined in Figure 5 is the computed c for $v = 1$ and pore p_1 at various times. At short times the concentration decreases rapidly near the pore and continues to decrease rapidly as the pore expands. At longer times the concentration remains significant in the vicinity distal from the expanding pore but decreases to small values at long times. For this value of v , the vesicle emptied most of its contents by $\tau = 2.6$, when the pore angle was approximately 2.6 radians. The corresponding efflux has a non-instantaneous rising phase and a decay phase that becomes exponential at long times, $\tau > 2.6$, after the efflux reaches 0.5% of its maximum. The maximum value of the efflux increases and the time to reach it decreases (Figure 6A-C) as v increases. The pore angle attains its maximum value of π after the maximum efflux is attained and the decay phase exhibits a discontinuity

between the maximum efflux and the onset of the decay phase. As expected, the decay phase becomes exponential at earlier times and is independent of v (Figure 6C).

Similar set of effluxes are shown for a pore whose radius expands linearly with time, pore p_2 (Figure 6D-F). Once again the magnitude of the efflux increases and the time to reach maximum efflux decreases with increasing non-dimensional velocity (Figure 6D and E). The spike shape is quite different from pore p_1 ; the rising phase is convex forming a cusp at its maximum with the pore angle reaching its maximum value of $\pi/2$ at the cusp (Figure 6D-E). The efflux decays exponentially beyond the cusp region and, similar to pore p_1 , the decay rate appears independent of v . The non-dimensional times τ_{\max} , $\tau_{1/2}^{\text{int}}$ and $\tau_{1/2}^{\text{spike}}$ are decreasing functions of v for both pores (Figure 7A-C). For small v , say $v < 0.2$, $p_1 \approx p_2$ and the respective effluxes are almost identical.

$\tau_{1/2}^{\text{int}}$ calculated with both numerical methods is in good agreement, they differ by 0.2 to 2% for the same value of v . The difference in the other times is more variable at 0.2 to 5%. This is because effluxes obtained with the above number of particles are noisy (Figure 7D-E). For pore p_2 , $\tau_{1/2}^{\text{spike}}$ exhibits the biggest discrepancy; this is related to the spike width which becomes very narrow as v increases. We found that this parameter is very sensitive to the number of elements in the mesh, the time step and the value of ε . Accurate values were not determined for v greater than seven at this resolution.

The dimensional time characteristics, $t_{1/2}^{\text{spike}}$, $t_{1/2}^{\text{int}}$ and t_{\max} , associated with Figure 7A-C can be fit to

$$t \propto \frac{R^n}{2^{2-n} D^{n-1} V^{2-n}}, \quad (4.3)$$

The exponents that achieve the least square error are tabulated (Table 1). They lie between 1 and 2 and decrease with increasing v . For $v < 0.2$ $n = 1.5$ for both pores (Figure 7, Table 1). This lower range is expected for exocytotic release from cells with vesicles of smaller size than those observed in mast cells of the beige mouse provided $RV < 2D$. The exponents for both pore P_1 and pore P_2 are different from a pore whose surface area expands at constant v , where the exponent n is always 2 (Appendix 3). Experimental observations show that the time characteristics of release grow as a power (less than 2) of the vesicle radius (Alvarez de Toledo *et al.* 1993 and Marszalek *et al.* 1996). This model, where molecules diffuse through a pore opening along the line of longitude, explains this observation.

To get a “rough” value of the pore velocity we use a best fit procedure to estimate V from the three time characteristics (Figure 2); the misfit is up to 30% for P_1 and P_2 except for $t_{1/2}^{\text{spike}}$ for P_2 where there is clearly no relationship. We determine velocities in the range 6 to 16 nmms⁻¹ for P_1 and 2 to 4 nmms⁻¹ for P_2 .

When we compare the experimental with the calculated we find that the effluxes are not identical (Figure 8). However, the “linear” opening functions do match some spike characteristics, e.g., the width and general shape of the experimental spike is expressed better by molecules escaping through pore P_1 whereas the initial rise of the experimental spike is better matched for molecules diffusing through pore P_2 .

We also show (Figure 8, left panel) that the experimental effluxes do not correspond to a pore that fully opens, i.e., for which $p(\tau)$ reaches π . In an attempt to consider more general opening functions we first show that the terminal opening angle of the pore, θ_{stop} ,

is obtainable from the exponential tail of the efflux. We do this with a simple modification of the p_1 introduced in (4.1). Namely, we consider

$$p_1^\#(\tau) \equiv \min(v\tau, \theta_{\text{stop}})$$

The family of curves for $v = 5$ are outlined in Figure 9 left panel. The slope varies with angle; it is steeper as the maximum angle subtending the pore increases and is independent of v . We compare the experimental effluxes with those calculated with this model ($p_1^\#$) in Figure 9 (middle panel) and find that it is still unable to mimic the experimental efflux, although the model more closely reproduces the decay phase. Assuming the measured decay phase (efflux at $> 1.5\text{s}$) represents pure diffusive flux, i.e., the pore has stopped expanding we calculate maximum pore angles between 60 to 85° (Figure 9 right panel) for the events shown in Figure 9 with an average angle of $70 (\pm 20)^\circ$ (averaged over 11 events). They were calculated assuming the vesicle radius had reached its maximum size i.e., it is about 1.4 times the initial radius of the vesicle (Marszalek *et al.* 1997b).

5. “Fast and Full” Opening

(Amatore *et al.* 1999) achieved excellent fits to effluxes of bovine chromaffin cells by assuming the pore opened completely *and* significantly faster than its contents were free to diffuse. They argued that such assumptions permitted them to approximate the efflux by the convolution of the flux from a fully open vesicle and the time rate of change of the pore’s relative surface area. That is, they supposed that

$$E(\tau) \approx \int_0^\tau \Phi(\tau - s) \sigma'(s) ds \quad (5.1)$$

where

$$\sigma(\tau) = \frac{1 - \cos p(\tau)}{2}$$

is the relative surface area of the pore and

$$\Phi(\tau - s) = -4\pi \frac{\partial U}{\partial r}(1, \tau - s)$$

where U is the concentration of the fully open vesicle. That is, U satisfies the initial-Dirichlet problem in the sphere

$$U_\tau = \Delta U, \quad U(r, \phi, \theta, 0) = 1, \quad U(1, \phi, \theta, \tau) = 0.$$

The great advantage of (5.1) is that it permits *direct* calculation of σ' and therefore p from measurement of E and prior calculation of U and Φ . Where (Amatore *et al.* 1999) compute U numerically via Brownian motion we note that separation of variables readily yields (Crank 1976, eqn. 6.18),

$$U(r, \tau) = \frac{2}{\pi} \sum_{n=1}^{\infty} \frac{(-1)^{n+1}}{n} \frac{\sin(n\pi r)}{r} \exp(-n^2\pi^2\tau) \quad (5.2)$$

and hence

$$\frac{\partial U}{\partial r}(1, \tau - s) = -2 \sum_{n=1}^{\infty} \exp(n^2 \pi^2 (s - \tau)) \quad (5.3)$$

With this explicit expression for Φ we may now construct an explicit discretization of the Volterra equation

$$E(\tau) = \int_0^{\tau} \Phi(\tau - s) f(s) ds. \quad (5.4)$$

We partition time in multiples of h , denote by T_k the piecewise linear hat function that is one at $\tau = kh$ and zero for $|\tau - kh| \geq h$, and express

$$E(\tau) = \sum_{i=1}^N j_i T_i(\tau) \quad \text{and} \quad f(\tau) = \sum_{i=1}^N f_i T_i(\tau) \quad (5.5)$$

Inserting these expressions in (5.4) and evaluating τ at kh we find

$$\begin{aligned} E_k &= \sum_{i=1}^N f_i \int_0^{\tau_k} \Phi(\tau_k - s) T_i(s) ds \\ &= 8\pi \sum_{i=1}^N f_i \sum_{n=1}^{\infty} \exp(-n^2 \pi^2 kh) \int_0^{kh} \exp(n^2 \pi^2 s) T_i(s) ds. \end{aligned} \quad (5.6)$$

Assembling the E_k and f_i into column vectors we recognize (5.6) to be a simple linear system of equations

$$E = \mathcal{V} f. \quad (5.7)$$

The components of the lower triangular Volterra matrix, \mathcal{V} , follow from explicit calculation of the latter integrals in (5.6). In particular, if $i < k$ then

$$\mathcal{V}_{k,i} = 8\pi \sum_{n=1}^{\infty} \frac{\exp(n^2 \pi^2 (i - k - 1)h) - 2 \exp(n^2 \pi^2 (i - k)h) + \exp(n^2 \pi^2 (i - k + 1)h)}{n^4 \pi^4 h}$$

while

$$\mathcal{V}_{k,k} = 8\pi \sum_{n=1}^{\infty} \frac{\exp(-n^2 \pi^2 h) + n^2 \pi^2 h - 1}{n^4 \pi^4 h}$$

With \mathcal{V} in hand we may now attempt to test the limits of the approximation (5.1). We accomplish this by supposing that p behaves like the p_1 in (4.1). In this case it follows that the derivative of the relative pore area is

$$\sigma'(\tau) = \begin{cases} v \sin(v\tau)/2 & \text{when } \tau < \pi/v \\ 0 & \text{when } \tau \geq \pi/v \end{cases} \quad (5.8)$$

We solve the full initial-boundary value problem, (2.8),(2.9),(2.12) with p as in (4.1) and then use the associated nondimensional efflux, E , as the left hand side in (5.7) and solve

for σ' . It is apparent that the σ' returned by (5.7) only begins to resemble the true σ' for v in excess of 5 (Figure 10).

We show in figure 8 that while $v \geq 5$ captures the rising phase of the experimental effluxes, the membrane does not completely flatten. Hence, for mast cells of the beige mouse the pore appears to be “fast” but not “full.” We also showed in §4 that it was not merely “fast” up to some $\theta_{\text{stop}} < \pi$. We must permit a larger class of opening functions.

6. “General” Opening

Recent theoretical evidence suggests that the pore radius should increase exponentially during final pore widening (Chizmadzhev *et al.* 2000) implying that pore velocity should increase with time during this stage. Therefore, we allowed the pore to expand under the condition that the velocity may change with time during the spike phase of release and found that we were able to simulate much more of the time course of the experimental efflux. We do this via solution of the least-squares problem

$$\min_p \int_0^\infty |E^{(m)}(\tau) - E(\tau; p)|^2 d\tau,$$

where $E^{(m)}$ denotes a normalized, nondimensional experimental efflux and $E(\tau; p)$ denotes the normalized value of (2.13). Three solutions, corresponding to three experimental events, are shown in Figure 11A-C, with the associated estimates for the pore radius, pore meridian, pore expansion rate and pore angle.

For the event shown in Figure 11A the velocity increased from about 1 to 18 nmms⁻¹ in the first 210 ms and then decreased from its maximum to zero when the pore radius reached its maximum value of 1.5 μm . As expected, there is little difference in the values between the meridian and the radius in the first 100 ms when pore angle is small. The expansion rate of the meridian increases to a maximum velocity of 21 nmms⁻¹ at 210 ms decreasing quickly to 12 nmms⁻¹ at 272 ms after which it decreases at a much slower rate to 10 nmms⁻¹ at 408 ms and then decreased to zero at 555 ms. For this event the calculated and experimental efflux were similar for 1s. Similar results were observed for the events in Figure 11B and C, except the initial velocity was constant for the first 50 to 70 ms, and the experimental efflux was simulated for first 500 and 750 ms. In all cases the exponential tail of the experimental efflux was difficult to reproduce. In general, for a vesicle of similar size R , the misfit increased as the times $t_{1/2}^{\text{int}}$ or $t_{1/2}^{\text{spike}}$ increased. Specifically, the fit was poor for events in Figure 2 that lie above the solid line; experimental efflux could not be reproduced beyond the peak maximum because the calculated efflux decreased much more quickly than the experimental. We suggest that these events were probably influenced by diffusional broadening from the release site to the fiber.

When we examine the time course of the radius during the initial rise in the velocity we find that the radius increases exponentially with time constant 82, 53 and 48 ms (Figure 10). We observed similar trends for the events shown in Figure 2A and B that lie on or below the fit to our model, and calculated average and median time constants of 82 (± 56 , averaged over 11 events) and 58 ms, respectively.

We found that the maximum pore angle ranged from 90 to 140° degrees and is much

greater than the maximum pore angle determined from the exponential decay phase (Figure 9 right panel).

7. Discussion

The efflux detected by a carbon fiber during exocytosis was calculated under the assumption that the release site (the vesicle) is a point source positioned at the edge of the cell with many molecules released instantaneously, diffusing within the surrounding medium and adsorbing onto the fiber (Schroeder *et al.* 1992, Haller *et al.* 1998). Simulations were used to predict the range of spike amplitudes and widths at half height as a result of simple diffusion from the release site to the sensor. For the case of release from chromaffin cells they showed that broadening alone could not account for the time course of the efflux, because it was always less than that observed experimentally. A second approach was to model release assuming the pore is cylindrical and either does not dilate (Khanin *et al.* 1994) or the pore radius expands linearly with time (Stiles *et al.* 1996. and Khanin *et al.* 1994)). We do not assume that the release site is a point source and show that it is not necessary to consider the time to diffuse through the neck, when D within the vesicle is much less than D through the neck (Figure 4). We also show that an efflux from a pore whose meridian or radius expands linearly with time, the “linear” opening cannot capture the time course of the experimental efflux from mast cells of the beige mouse (Figure 8). Because the pore does not appear to reach π we conclude that it is also not possible to use the “fast and full” pore of Amatore *et al.* (1999). We therefore propose a more “general” description of the inverse problem which appears to simulate much more of the efflux than the “linear” case. With respect to our uniqueness result of §3 we note that in the large literature on recovering coefficients in parabolic equations (Jones 1963 and Isakov 1998) the problem of recovering a time varying function on the boundary has not been addressed. We expect that our assumption of analyticity is merely technical and so expect stronger versions of our uniqueness result. Throughout our analysis we make the tacit assumption that the radius of the granule does not change during spike phase of release. This assumption is not perfectly valid, because the granule matrix swells during release, i.e., R is also a function of time. We now examine the limitations of this and other assumptions.

Expansion of the Secretory Granule Matrix

In mast cells the surface area of the granule matrix expands by about 2 times during release (Marszalek *et al.* 1997b). This arises because serotonin and other molecules are released through exchange with counter-ions, mainly sodium in the extracellular milieu. This exchange increases the repulsive forces within the polymer network and the gel matrix swells as water enters the vesicle. To obtain a better estimate of P (Figure 11) would require revision of the model by solving the diffusion equation in three dimensions with both a moving mesh and moving boundary and coupling transport equations with the mechanics of gel expansion. Experiments would need to be obtained where the expansion of the gel is monitored at high temporal and spatial resolution and release and fusion measured simultaneously with amperometry and admittance; both the irregular shape of the vesicles from mast cell of beige mouse (Marszalek *et al.*, 1997a) and expansion of the gel would then be considered. The values (Figure 11) for pore expansion rate serve as first estimate

for this parameter and we suggest that those obtained during the initial phase (50 to 200 ms) are reasonable estimates because gel matrix has not expanded significantly in this time frame (Marszalek *et al.* 1997b). In this period, the radial velocity usually increased from 0 to 7 (± 4) nmms⁻¹ the velocity remained unchanged for the next 20-100 ms after which the radius increased exponentially to a maximum velocity of 20 (± 7) nmms⁻¹ (median 19 nmms⁻¹) with the maximum meridian velocity of 23.9 (± 6) nmms⁻¹ (median 23.5 nmms⁻¹) (Figures 11 and 12). These velocities are much slower than those predicted by Amatore *et al.* (2000) for fusion pore expansion for bovine chromaffin cells. They also did not consider matrix expansion in their calculations, but assumed that the gel expanded to its maximum value at the onset of the spike phase. From their opening functions (Amatore *et al.* 2000, their Figure 1, and average diffusivity, 4×10^{-8} cm²s⁻¹) we determined that the average rate of pore expansion was significant between 50 to 175 nmms⁻¹. As illustrated, this has to be the case for their analysis to be valid (Figure 10). This suggests that during the spike phase of release from chromaffin granules that the fusion pore explodes or bursts. We did not determine this for mast cells of the beige mouse, our first estimate suggest that it expands at 5 to 7 times less and that the pore angle rarely reaches π before the contents are released (Figure 9 left panel). We found that the pore angle determined from the exponential decay of the efflux (Figure 9, right panel) was much smaller than that determined from the general pore model (cf. Figure 11 3rd panel). Because the former was calculated from the exponential decay which presumably represents pure diffusive flux and gel expansion was also considered we suggest that the smaller value at 70 (± 20) $^\circ$ is the better estimate. During in vitro monitoring of exocytosis from mast cells of the beige mouse with patch clamp amperometry one (1) or no (0) granules are found sticking to the outside of the cell at the end of an experiment. This contrasts similar experiments with chromaffin granules where many granules are observed extruding from the vesicles and lying outside the cell at the end of an event, so it is possible that higher velocities are attained in this system. We suggest (cf. Amatore *et al.* 2000) that the easiest way to determine if the pore has flattened into the membrane, i.e., if p reaches π , is to examine the exponential rate of the decay phase. If this rate agrees with the least eigenvalue of the Dirichlet Laplacian on the 3-ball then the pore has indeed flattened. We note that if the “fast and full” pore is applicable to other endocrine cells and neurons that the pore would attain velocities in excess of 30, 125 and 220 nmms⁻¹ for rat mast cells (R: 350 nm), rat chromaffin cells (R: 80 nm) and dense core vesicles found in neurons (R: 45 nm), assuming a D of 2×10^{-8} cm²s⁻¹.

Analysis predicts that for flaccid membranes (zero tension) the radius should increase linearly with time as pore widens; the driving force in this case is the negative spontaneous curvature of the participating lipids (Chizmadzhev *et al.*, 1995). In the case where tension is greater than zero, the radius increases exponentially with total tension as the driving force (Chizmadzhev *et al.* 1995 and Chizmadzhev *et al.* 2000). We observe an initial jump in the radius followed by a linear and exponential rise. We suggest that increased tension in the system is caused by gel expansion, i.e. tension increases as water enters and the gel starts to expand. This increased tension drives pore widening. Therefore, we suggest that although pore dilation occurs in the absence of osmotic swelling (Monck *et al.* 1991) that gel expansion affects the rate of pore expansion especially during the spike phase of

release. This is similar to that expressed by Chizmadzhev *et al.*, (2000) and Amatore *et al.* (2000) and can be tested by considering gel expansion in the analysis. The velocity decreased at times greater than 200 ms, (Figure 11). It is probable that velocity should increase and then decrease; as efflux proceeds tension will decrease until it is eventually counteracted by frictional and viscous forces. The result of which is to diminish membrane and gel movement.

Constant Diffusivity

We simulate the data with D determined from isolated granules at $2 \times 10^{-8} \text{ cm}^2\text{s}^{-1}$ and suggest that this slower D is more appropriate to use at this stage. We conclude this because the conductance calculated from the admittance (Nanavati *et al.* 1992) was immeasurably large during the initial rise of the spike. If the D was 14 times faster as measured from the foot phase of release ($2.9 \times 10^{-7} \text{ cm}^2\text{s}^{-1}$, Marszalek *et al.* 1997b) we calculate that the pore radius should range from 10 to 15 nm in the first 75 ms, which would result in a measurable conductance of 13 nS. This contrasts a conductance of 200 nS for pore radius of 150 to 200 nm calculated for the slower D in the same 75 ms time period. However conductance calculations are very sensitive to small magnitudes of the real part of the admittance found at this stage of a fusion event (Nanavati *et al.* 1992). To obtain a more definitive test it would be useful to conduct high frequency admittance measurements (Albillos *et al.* 1997) where more accurate conductance values could be obtained. Our analysis cannot determine definitively which diffusion coefficient is the more appropriate one to use, results suggests that it is probably not constant (see below).

The “general” pore model failed to capture the tail of the efflux (Figure 11). We examined the possibility that it could represent the first stages of “resealing” of the cell (Nielsen *et al.*, 1981 and Steyer *et al.* 1997), but found that pore contraction caused the efflux to decrease at a faster, not a slower rate. There is a difference of about 1.2 pH units between the interior of the vesicle (pH 6.0) and extracellular solution (Johnson *et al.* 1980) and since binding to heparin, at least for histamine, depends upon pH (Rabenstein *et al.* 1992) it is expected that D will vary during the release process as the pH gradient equilibrates. In addition, there is evidence that D would increase (not decrease) by about a factor of 2 as the gel expands and the network becomes less tortuous (Krizaj *et al.*, 1996 and Rusakov and Kullmann 1998). However a slow decaying efflux indicates decreasing (not increasing) diffusivity and suggests that components of the matrix other than heparin proteoglycan might bind serotonin more effectively at pH 7.2 (cf pH 6.0). Indeed, in contrast to others (Amatore *et al.* 2000) preliminary analysis of the foot component of release from mast cells of the beige mouse (data not shown) suggests that the diffusivity may be faster during this phase.

Finite Size of Transmitter Molecules

Our analysis does not consider that the molecule has a finite size, because it is not significant for release from vesicles of this size. By the first time step, the diameter of the pore (2 x pore radius) is much greater (10 to 20 times) than 0.8 nm, approximate size of small transmitter molecule.

Broadening of Signal

In our calculations, we assume that the fiber lies at the matrix-solution interface (Figure 3C), we do not consider the additional time required to diffuse throughout the

extracellular solution. We calculate that broadening of the signal should only impact results when the distance from the source to the detector is 2-3 μm , assuming diffusivity is close to the bulk in the extracellular medium. We found for events that originated from vesicles of similar size that the misfit increased as the times $t_{1/2}^{\text{int}}$ and $t_{1/2}^{\text{spike}}$ increased, with poor fits to the model for events that lie above the solid lines in Figure 2A and 2B. We suggest that this discrepancy occurs with cases where vesicles are a significant distance from the detector i.e., similar in size to the fusing vesicle.

Concentration is initially uniform throughout the vesicle

We assume that the concentration of serotonin is uniform throughout the vesicle. This infers that the binding moieties for serotonin on heparin proteoglycan and the other binding proteins within the vesicle are uniformly distributed. We were unable to find any evidence that supports or refutes this assumption. We used it because it provides for the most straightforward initial condition. We note that this assumption is less valid when there is significant leakage from the vesicles and/or if there were multiple transient release events that went undetected prior to the spike phase.

8. Conclusions

1. A pore that expands along the line of longitude of a spherical vesicle can explain the reported relationship that time of release grows as a power (less than 2) of the vesicle radius, R .
2. A pore whose radius or meridian expands linearly “linear” opening or a pore that expands very quickly flattening into the membrane “fast and full” opening do not reproduce the time course of the efflux from mast cells of the beige mouse. A larger class of opening functions was required to reproduce the efflux.
3. We establish that the pore does not completely flatten into the membrane, $P < \pi$, and estimate a maximum angle of $70(\pm 20)^\circ$. We found that in the first 50-200 ms of the efflux that the pore radius increases exponentially with a time constant of $82(\pm 62)$ ms with the pore expansion rate reaching a maximum velocity of $20 (\pm 7) \text{ nmms}^{-1}$ (radius) and $24 (\pm 6) \text{ nmms}^{-1}$ (meridian).
4. This model is suitable to describe exocytotic release from other cells and neurons provided that D of the secretory product within the vesicle is much less than D within the pore neck.
5. Better estimates of P will require adoption of improved models that couple transport equations with mechanics of gel expansion. This modeling should be performed in conjunction with more precise experimentation where expansion of the gel, release, and fusion are monitored simultaneously at high spatial and temporal resolution, and broadening of the amperometric signal is reduced by use of smaller diameter probes.

9. Acknowledgements

Experimental data for mast cells of the beige mouse was obtained at The Mayo Clinic Rochester, Minnesota, USA. We are grateful to J.M. Fernandez for his encouragement during the early stages of this work. The work of B.F. was supported by Keck Center for Computational Biology, Rice University under NLM training grant ITI5LM07093. The

work of S.C. was partially supported by NSF Grant DMS-0077728.

10. References

Albillos A., G. Dernick, H. Horstman. W. Almers G. Alvarez de Toledo and M. Lindau. 1997. The exocytotic event in chromaffin cells revealed by patch amperometry. *Nature* 389:509-512.

Alvarez de Toledo., G.,R. Fernandez-Chacon and J.M. Fernandez. 1993. Release of secretory products during transient vesicle fusion. *Nature* 363: 554-557.

Amatore C., Y. Bouret and L. Midrier. 1999. Time-resolved dynamics of vesicle membrane during individual exocytotic secretion events as extracted from amperometric monitoring of adrenaline exocytosis by chromaffin cells. *Chem. Eur. J.* 5: 2151-2162.

Amatore C., Y. Bouret, E.R. Travis and R.M. Wightman. 2000. Interplay between membrane dynamics, diffusion and swelling pressure governs individual vesicular exocytotic events during release of adrenaline by chromaffin cells. *Biochimie* 82: 481-496.

Bruns D. and R. Jahn. 1995. Real-time measurement of transmitter release from single synaptic vesicles. *Nature* 377:62-65.

Bruns D., Riedel D., Klingauf J. and R. Jahn. 2000. Quantal release of serotonin. *Neuron* 28:205-220.

Curran M.J., F.S. Cohen, D.E. Chandler, P.J. Munson and J. Zimmerberg. 1993. Exocytotic Fusion Pores Exhibit Semi-Stable States. *J. Membr. Biol.* 133:61-75.

Chandler D.E. and J.E. Heuser. 1980. Arrest of membrane fusion events in mast cells by quick freezing. *J. Cell Biol.* 86:666-674.

Chizmadzhev Y.A., F.S. Cohen, A. Scherbakov and J. Zimmerberg. 1995. Membrane mechanics can account for fusion pore dilation in stages. *Biophys. J.* 69: 2489- 2500.

Chizmadzhev Y. A., P.I. Kuzmin, D.A. Kumenko, J. Zimmerberg and F.S. Cohen. 2000. Dynamics of fusion pores connecting membranes of different tensions. *Biophys. J.* 78: 2241-2256.

Crank, J. 1976. *The Mathematics of Diffusion.* Oxford University Press, Oxford UK.

Demmel J.W., S. C. Eisenstat, J.R. Gilbert, X. S. Li and J.W.H. Liu. 1999. A supernodal approach to sparse partial pivoting. *SIAM J. Matrix Anal. Appl.* 20: 720-755.

Dvorak A.M., I. Hammel and S. J. Galli. 1987. Beige mouse mast cells generated *in vitro*: ultrastructural analysis of maturation induced by sodium butyrate and IgE-mediated antigen dependent degranulation. *Int. Archs Allergy appl. Immun.* 82: 261-268.

Fisher R.J., J. Pevsner and R.D. Burgoyne. 2001. Control of fusion pore dynamics during exocytosis by Munc18. *Sci.* 291:875-878.

Friedman, A. 1964. *Partial Differential Equations of Parabolic Type.* Prentice-Hall, Englewood Cliffs, N.J.

Graham M.E. and R.D. Burgoyne. 2000. Comparison of cysteine string protein (Csp) and mutant α -SNAP overexpression reveals a role for Csp in late steps of membrane fusion in dense-core granule exocytosis in adrenal chromaffin cells. *J. Neurosci.*20:1281-1289.

Haller M., C. Heinemann, R.H. Chow, R. Heidelberger and E. Neher. 1998. Comparison of secretory responses as measured by membrane capacitance and by amperometry. *Biophys. J.* 74:2100-2113.

Isakov, V. 1998 Inverse Problems for Partial Differential Equations, Springer, New York.

Johnson R.G., S.E. Carty, B.J. Fingerhood and A. Scarpa. 1980. The internal pH of mast cell granules. FEBS Lett. 120:75-79.

Jones, B.F. Jr. 1963 Various methods for finding unknown coefficients in parabolic differential equations. Comm. Pure Appl. Math. 16 33-44.

Khanin R. H. Parnas and L. Segel. 1994. Diffusion cannot govern the discharge of neurotransmitter at fast synapses. Biophys. J. 67:966-972.

Krizaj D. M.E. Rice, R.A. Wardle and C. Nicholson. 1996. Water compartmentalization and extracellular tortuosity after osmotic changes in cerebellum of *Trachemys scripta*. J of Physiol. 492: 887-896.

Marszalek P.E., B. Farrell and J.M. Fernandez. 1996. Ion exchange gel regulates neurotransmitter release through the exocytotic fusion pore. In Organellar Ion Channels and Transporters, Vol. 51. D.E. Clapham and B.E. Ehrlich, editors, 211-222.

Marszalek P.E., B. Farrell, P. Verdugo and J.M. Fernandez. 1997a. Kinetics of release of serotonin from isolated secretory granules. I. Amperometric detection of serotonin from electroporated granules. Biophys. J. 73:1160-1168.

Marszalek P.E., B. Farrell, P. Verdugo and J.M. Fernandez. 1997b. Kinetics of release of serotonin from isolated secretory granules. II. Ion-exchange determines the diffusivity of serotonin. Biophys. J. 73: 1169-1183.

Monck J.R., A.F. Oberhauser and J.M. Fernandez. 1991. Is swelling of the secretory granule matrix the force that dilates the exocytotic fusion pore? Biophys. J. 59: 39-47.

Nanavati C., V.S. Markin, A.F. Oberhauser and J.M. Fernandez. 1992. The exocytotic fusion pore modeled as a lipidic pore. Biophys. J. 63: 1118-1132.

Nielsen E.H., P. Bytzer, J. Clausen and N.Chakravarty. 1981. Electron microscopic study of the regeneration *in vitro* of rat peritoneal mast cells after histamine secretion. Cell Tissue Research 216: 635-645.

Rabenstein D.L., P. Bratt and J. Peng. 1998. Quantitative Characterization of the binding of histamine to heparin. Biochemistry. 37: 14121-14127.

Rabenstein D.L., P. Bratt, T. D. Schierling, J. M. Robert and W. Guo. 1992. The interaction of biological molecules with heparin and related glycosaminoglycans. 1. Identification of a specific binding site for histamine. J. Am. Chem. Soc. 114: 3728-3285.

Rusakov D.A. and D.M. Kullmann. 1998. Extrasynaptic glutamate diffusion in the hippocampus: ultrastructural constraints, uptake and receptor activation. J. Neuroscience 18:3158-3170.

Schroeder T.J., Jankowski, K.T. Kawagoe, R.M. Wightman, C. Lefrou and C. Amatore. 1992. Analysis of diffusional broadening of vesicular packets of catecholamines released from biological cells during exocytosis. Anal. Chem. 64: 3077-3083.

Schroeder T.J., R. Borges, J.M. Finnegan, K. Pihel, C. Amatore and R.M. Wightman. 1996. Temporally resolved independent stages of individual exocytotic secretion events. Biophys. J. 70: 1061-1068.

Spruce A.E., L.J. Breckenridge, A.K. Lee and W. Almers. 1990. Properties of the fusion pore that forms during exocytosis of a mast cell secretory vesicle. Neuron 4: 643-654.

Steyer J.A., H. Horstmann and W. Almers. 1997. Transport, docking and exocytosis of single secretory granules in live chromaffin cells. *Nature* 388: 474-478.

Stiles J.R., D. Van Helden, T.M. Bartol, Jr, E. E. Salpeter and M.M. Salpeter. 1996. Miniature endplate current rise times $< 100 \mu s$ from improved dual recordings can be modeled with passive acetylcholine diffusion from a synaptic vesicle. *Proc. Natl. Acad. Sci.* 93:5747-5752.

Urena. J.R. Fernandez-Chacon A.R., A.R. Benot, G. Alvarez de Toledo and J. Lopez-Barneo 1994. Hypoxia induces voltage dependent Ca^{2++} entry and quantal secretion in carotid body glomus cells. *Proc. Natl. Acad. Sci.* 91: 10208-10211.

Uvnas, B. and C-H. Aborg. 1977. On the cation exchanger properties of rat mast cell granules and their storage of histamine. *Acta physiol.scand.* 100: 309-314.

Uvnas B. C-H. Aborg, L. Lyssarides and J. Thyberg. 1985. Cation exchanger properties of isolated rat peritoneal mast cell granules. *Acta. Physiol. Scand.* 125: 25-31.

Yurt R.W, R.W. Leid, Jr, K.F. Austen and J.E. Silbert. 1976. Native heparin from Rat peritoneal mast cells. *J. Biol. Chem.* 252: 518-521.

Zhou Z. and S. Mislser. 1995a. Action potential-induced quantal secretion of catecholamines from rat adrenal chromaffin cells. *J. Biol. Chem.* 270:3498-3505.

Zhou Z. and S. Mislser. 1995b. Amperometric detection of stimulus-induced quantal release of catecholamines from cultured cervical ganglion neurons. *Proc. Natl. Acad. Sci.* 92: 6938-6942.

Zimmerberg J., M. Curran, F.S. Cohen and M. Brodwick. 1987. Simultaneous electrical and optical measurements show that membrane fusion precedes secretory granule swelling during exocytosis of beige mouse mast cells. *Proc. Natl. Acad. Sci.* 84:1585-1589.

11. Figure Legends

Figure 1. Simultaneous experimental measurement of membrane fusion and the spike phase of release of 5-HT from mast cells of the beige mouse. (A) Typical data showing the imaginary component of the cell membrane admittance and (B) current recorded at carbon fiber electrode for mast cells undergoing exocytosis. The time constants are defined where t_{\max} , $t_{1/2}^{\text{int}}$, $t_{1/2}^{\text{spike}}$ for the first and second spike are 230, 433 and 290 380, 548 and 340 ms, respectively. The delay between onset of fusion (admittance step) and spike phase of release of 5-HT is 30 and 77 ms, respectively. The radius of the granule associated with spike one and two are 1.2 and 1.5 μm respectively. (C) The second spike and time course of the integral is normalized and shown at higher magnification.

Figure 2. Plots of radius of granules against time at which one half of the 5-HT molecules are released, $t_{1/2}^{\text{int}}$ (A); width of the spike at half maximum, $t_{1/2}^{\text{spike}}$ (B) and time to reach maximum efflux, t_{\max} (C). The solid and dashed lines are the fits of the data to pore P_1 , and P_2 , where velocity (V) is determined by minimizing a misfit function for each time characteristic. In this analysis we include events that are independent, but exclude spikes that exhibit pre-spike features, spikes that overlapped or incomplete spikes. The latter were usually evident when the time course of the integral did not plateau (c.f. Figure 1C). Twenty-two events from 11 cells fit these criteria, which is less than one half of the total singular events (n=53) recorded from these cells. The delay, as measured by difference between onset of admittance (imaginary component) and amperometric signals, was sometimes close to resolution of recordings at < 30 ms. Less than one half of the events (10) exhibit a delay of < 300 ms, and is similar to that reported (Alvarez de Toledo *et al.* 1993) for events where no foot was observed. The rest of the events exhibited delays that were greater with a maximum at ≈ 2000 ms.

Figure 3. Geometry of the exocytotic fusion pore. (A) Pore shaped like an hourglass shown with spherical vesicle attached. (B) Coordinates of the pore modeled where R is the radius of the vesicle and θ the angle that subtends the pore. (C) Pore expansion along the line of longitude of vesicle where pore P_1 opens to π i.e., up to (v) pore, P_2 opens to $\pi/2$, i.e., up to (iii).

Figure 4. Justification for not including the time to diffuse through pore neck when modeling release from endocrine cells, like mast cells of the beige mouse. (A) Time to empty neurotransmitter molecules from a vesicle of R, 20 nm when the diffusivity through the neck and vesicle are assumed to be the same at $6 \times 10^{-6} \text{ cm}^2\text{s}^{-1}$ and the numbers adjacent to plots indicate length of a cylindrical pore neck. The concentration, (C) is normalized (c) relative to initial concentration, (C_0) in vesicle. The plot marked zero was calculated numerically by finite element method with equation (2.8) under the initial and boundary conditions (2.9) and (2.12). In this calculation, the radius of the pore increases linearly at a velocity of 25 nmms^{-1} while molecules diffuse within the vesicle at $6 \times 10^{-6} \text{ cm}^2\text{s}^{-1}$. The initial radius of the pore was assumed to be 0.93 nm. The time to empty the vesicle through a pore with neck 5 and 10 nm long was determined with the approximate analytical expression outlined by Khanin and colleagues (Khanin *et al.* 1994 their equation 3) using the same parameters. Although this expression underestimates the time to empty

a vesicle (Stiles *et al.* 1996) this is insignificant relative to the much longer time molecules take to escape when the diffusivity of transmitter is up to 300 times slower relative to its bulk value. (B) Same as in (A) except the diffusivity within the vesicle is $2.9 \times 10^{-7} \text{ cm}^2\text{s}^{-1}$ (plot marked 0 nm) and $2.0 \times 10^{-8} \text{ cm}^2\text{s}^{-1}$ (inset, plot marked 0 nm). (C) Same as in (B) except pore velocity is 0.35 nmms^{-1} in all simulations.

Figure 5. Concentration within the vesicle is affected by the expansion of the pore. (A) Spatial distribution of concentration at nine (9) times for $v = 1$ and pore p_1 where τ is given above each plot and corresponds to the nine open circles shown in A. (B) Calculated efflux and time course of integral for $v = 1$ and pore p_1 . The values for τ_{\max} , $\tau_{1/2}^{\text{int}}$ and $\tau_{1/2}^{\text{spike}}$ are, 0.992, 1.039 and 1.373.

Figure 6. As v increases the maximum efflux increases and the time course of the efflux is faster. (A) Calculated effluxes for pore p_1 for v ranging from 0.6 to 3.4, with v increasing by increments of 0.2. (B) Efflux for higher v values including v at 5, 7, 10, 13, 15, 20 and 25. (C) Log plot of the decay phase of the efflux. The vertical lines note the time when the angle reaches π . (D), (E) and (F) same as (A), (B), and (C), except pore is p_2 and angle reaches $\pi/2$ at the maximum.

Figure 7. Comparison of the results determined by finite element and monte carlo methods. Plots of τ versus v for three times (A-C) and efflux calculated for p_1 (D) and p_2 (E) for $v = 25$. Solid circles: FE, p_1 , open circles: MC, p_1 solid triangles: FE, p_2 , open triangles: MC, p_2 . The solid and dashed line represents efflux determined by FE and MC. The efflux calculated by MC is average of 10 (D) and 20 (E) simulations, respectively.

Figure 8: Comparison of the experimental efflux (open circles) with that calculated for “linear” opening (solid lines). A and B are the experimental spikes shown in Figure 1C, and 1A (smaller spike) and C is a release event from a second cell. The radius and delay for this spike are $1.54 \mu\text{m}$ and 1540 ms respectively.

Figure 9. Decay of the slope depends upon the maximum angle that subtends the pore. Spikes calculated for pore p_1 where θ_{stop} in order of decreasing slope is 180, 150, 130, 110, 90, 70 and 50° (left panel). Comparison of model (solid lines) with experiment (open circles) (middle panel). Experimental decay phase (gray lines) is compared with calculated decay phase (black lines) (right panel). The maximum angle is indicated and was calculated with a D of $2 \times 10^{-8} \text{ cm}^2 \text{ s}^{-1}$ and assuming secretory gel was in its expanded state.

Figure 10. Assessing the “fast and full” approximation. Comparison of the actual σ' (solid) with the recovered σ' (dashed) at several v .

Figure 11. Least-square fit of the time course of the experimental efflux for mast cells of the beige mouse. The fit was obtained by the `lsqnonlin` function in Matlab using finite difference gradients. From these simulations we determine the size of the pore, the velocity of pore expansion and pore angle. The symbols represent: open circles: experimental efflux, closed circles: calculated efflux; solid diamonds: radius of pore; open diamonds: meridian of pore, (second panel); open triangles: pore angle (third panel); solid

squares: pore expansion rate of pore radius; open squares: pore expansion rate of meridian (fourth panel). The solid and dashed lines in 4th panel are drawn as a guide to the eye.

Figure 12. A semi-log plot of pore radius versus time. A, B and C refer to spikes shown in Figure 11. Radius of the pore during initial pore expansion is plotted up to time where velocity angle reached maximum (Figure 11, 4th panel). The dashed lines are fits to the exponentially increasing function over the period when velocity increased. Time constants were determined to be: 82, 53 and 48 ms.

12. Appendix 1: Experimental Methods

Peritoneal mast cells were isolated from the beige mouse (b_g^j/b_g^j , Jackson Laboratories, Bar Harbour, ME) following procedures described (Nanavati *et al.* 1992). Briefly, cells were obtained by peritoneal lavage by use of CO₂ independent medium with 1% bovine serum albumin (fatty acid free; ICN Biomedicals, Aurora, OH) dissolved. This suspension was centrifuged at 100 x g for ten minutes and then plated on glass bottomed chambers and stored at 37° C under 5% CO₂.

During patch clamp experiments the solution within the pipette contained (in mM) 140 K-glutamate, 7 MgCl₂, 3 KOH, 0.2 ATP, 1 CaCl₂, 10 EGTA, 10 HEPES (pH 7.2,) and 0.01 GTP γ S and the extracellular solution contained : 150 mM NaCl, 2 CaCl₂, 1 MgCl₂, 1.5 NaOH, 2.8 KOH, 10 HEPES (300 mOsm/kg, pH 7.2). Cell membrane admittance was measured with the patch-clamp technique in the whole-cell mode. A detailed description of the technique and calculations are described in Nanavati *et al.* 1992 and Marszalek *et al.* 1997b. The capacitance of a granule was determined by measuring the stepwise change in the imaginary part of the admittance detected during an exocytotic event. The admittance measurements were collected at 104 Hz. The radius, R of the granule was calculated assuming it is spherical with the specific membrane capacitance of $0.57 \mu\text{Fcm}^{-2}$ (Zimmerberg *et al.* 1987).

Carbon fiber electrodes (Thornel P-55; Amoco Corp., Greenville, SC nominal radius 5 μm) were prepared as described (Marszalek *et al.* 1997a). During an experiment the fiber was placed over the cell $< 1\mu\text{m}$ from its apex. The electrode was held at +0.65 volts versus Ag/AgCl reference electrode. The current was amplified by an EPC-7 (List Electronics, Darmstadt, Germany) patch clamp amplifier and collected at 104 Hz. A computer program written in LabView (v3.1) for Windows in conjunction with a DAQ card (AT-MIO-1 6X) controlled the acquisition of the admittance and amperometric measurements.

13. Appendix 2: Numerical Methods

Finite Elements and Backward Euler. With the specification of p the full system, (2.8),(2.9),(2.12) may be readily solved by finite elements in space and finite differences in time. With respect to space we build a staggered rectilinear mesh by partitioning

$$0 = \rho_1 < \rho_2 < \dots < \rho_{N_r} = 1 \quad \text{and} \quad 0 = \theta_1 < \theta_2 < \dots < \theta_{N_\theta} = \pi$$

and so arrive at a grid with $N = N_r \times N_\theta$ nodes at the points (ρ_i, θ_j) . In order to capture the behavior at the pore the partition in ρ was coarse for small i and fine for large i while

the partition in θ was fine for small j and coarse for large j with the cutoff between large and small determined by the rate at which the pore was opening. We number the nodes from 1 to N and denote by $h_k(\rho, \theta)$ the bilinear hat function that is 1 at the k th node and zero at all others. We insert the approximation

$$c(\rho, \theta, \tau) = \sum_{k=1}^N a_k(\tau) h_k(\rho, \theta)$$

in (2.8), multiply across by h_j and integrate over $[0, 1] \times [0, \pi]$ and so arrive at an initial value problem for $a = [a_1 \ a_2 \ \cdots \ a_N]$, namely

$$Ma'(\tau) = K(\tau)a(\tau), \quad a(0) = 1.$$

This system is easily and efficiently solved via Backward Euler, with timestep $d\tau$,

$$(M + d\tau K(\tau + d\tau))a(\tau + d\tau) = Ma(\tau) \tag{13.1}$$

because M and $K(\tau)$ are symmetric, positive definite and zero outside a band whose half-width is N_r . We worked on grids for which N was between 10 and $20K$, the pore resistance, ε , was between 10^{-4} and 10^{-8} , and the regularization parameter δ in (2.12) was zero. We use the sparse matrix package SuperLU in the solution of (13.1), (Demmel *et al.* 1999, www.nersc.gov/~xiaoye/SuperLU/).

Monte Carlo. We use the full (2.1)–(2.4) to calculate the efflux and estimate $t_{1/2}^{\text{int}}$, t_{max} and $t_{1/2}^{\text{spike}}$ by the Monte Carlo method. In comparison to the finite element method we work in three spatial dimensions and in the original dimensioned variables. The pore geometry and boundary conditions (2.4) are identical to that described (Figure 3). Briefly, at time $t = 0$,

$$500, 1250, 4000, 6750, 8000, 15625, 31500 \quad \text{and} \quad 37500$$

particles were placed uniformly into spheres of radius 5, 7, 10, 15, 20, 25 and 30 nm, respectively. The particles are infinitely small and described by spherical coordinates. At $t > 0$ particles move together and time is calculated with $j\langle l \rangle^2/6D$, where j is the number of steps and l the step length. The step length was at least fifty times smaller than R and terminates when all of the particles diffuse through the pore. For pore P_2 the step length was always 100 times smaller than the radius and the number of particles doubled. We found we had to average about 10 and 25 simulations to achieve comparable noise level to that obtained by the FE method.

14. Appendix 3

We examine the efflux produced by a pore whose surface area grows at constant velocity V (m^2s^{-1}). In the language of (2.3) this pore is

$$\{(R, \phi, \theta) : 0 \leq \phi < 2\pi, 0 \leq \theta \leq \pi, 2\pi R^2(1 - \cos \theta) \leq Vt\}. \tag{14.1}$$

In the new variables,

$$\rho \equiv \frac{r}{R}, \quad \tau \equiv \frac{Dt}{R^2}, \quad \text{and} \quad v \equiv \frac{V}{2D} \quad (14.2)$$

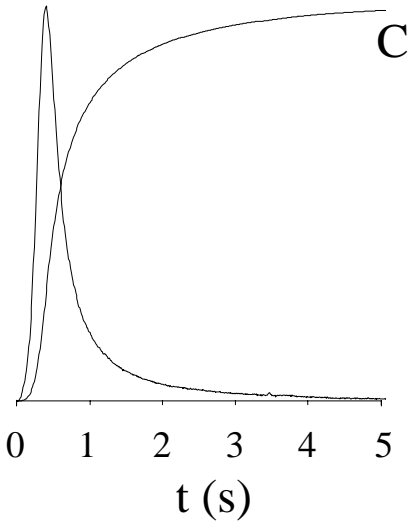
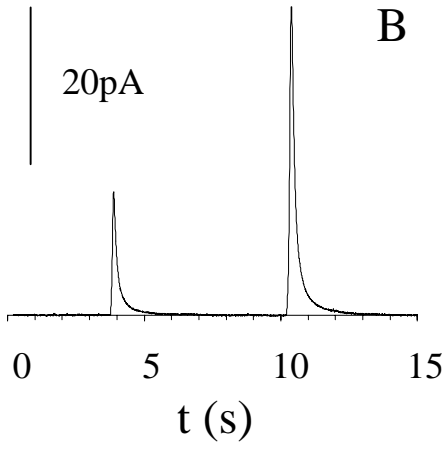
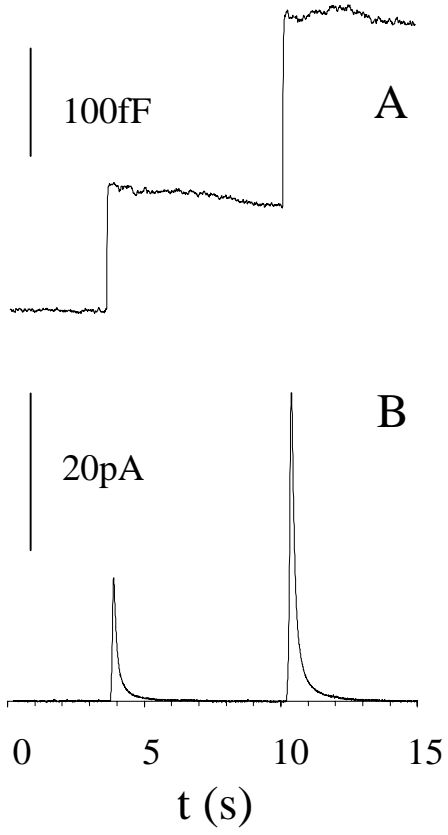
this becomes

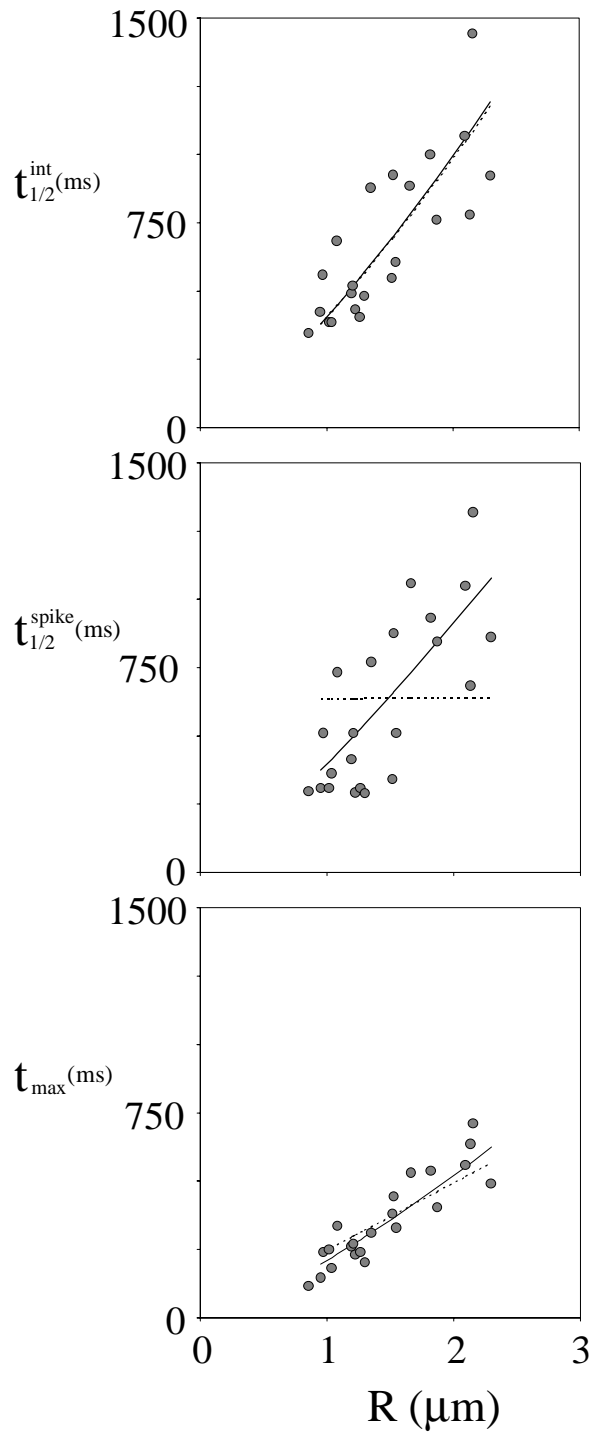
$$\{(\rho, \phi, \theta) : 0 \leq \phi < 2\pi, 0 \leq \theta \leq \pi, \pi(1 - \cos \theta) \leq v\tau\}. \quad (14.3)$$

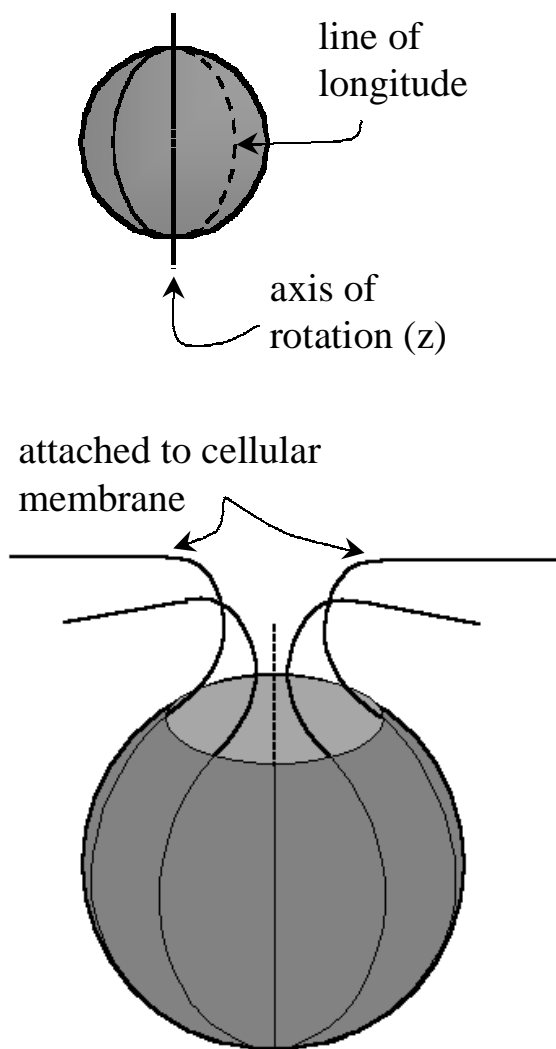
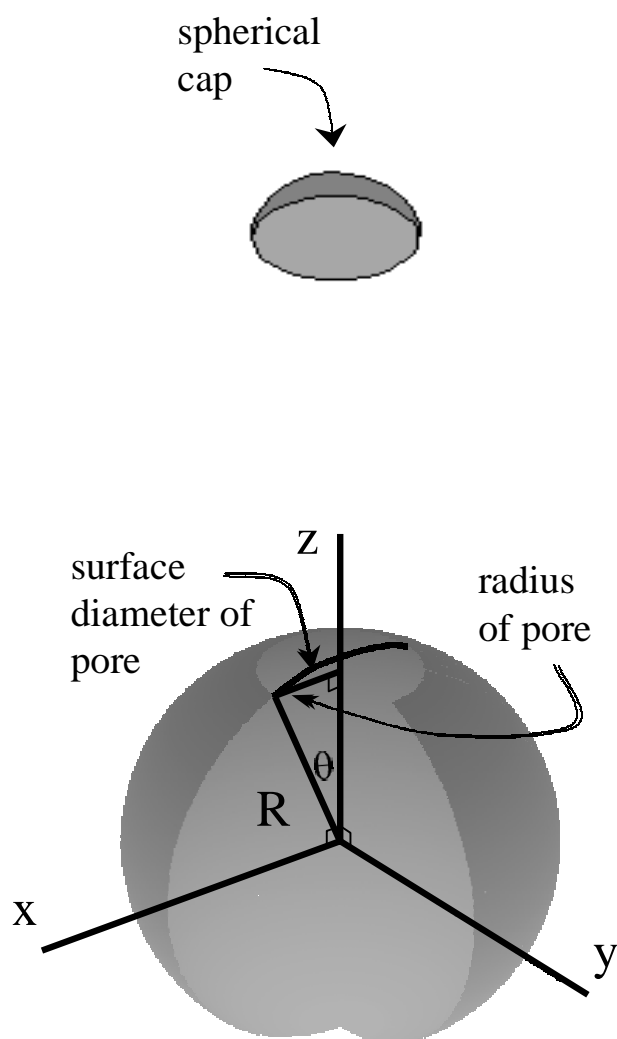
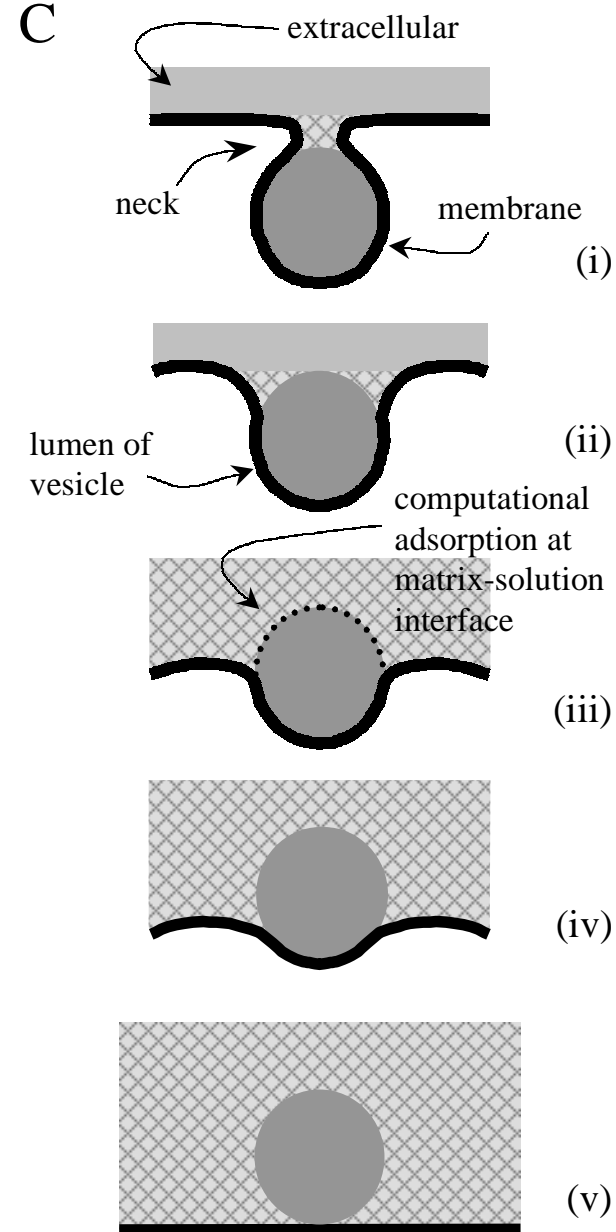
We stress the fact that the vesicle radius, R , appears in (14.3) *only* through its role in τ . As a result, the nondimensional time characteristics of the efflux associated with this pore will be *independent* of R . The resulting dimensional time characteristics will therefore, following (14.2), each be proportional to R^2 .

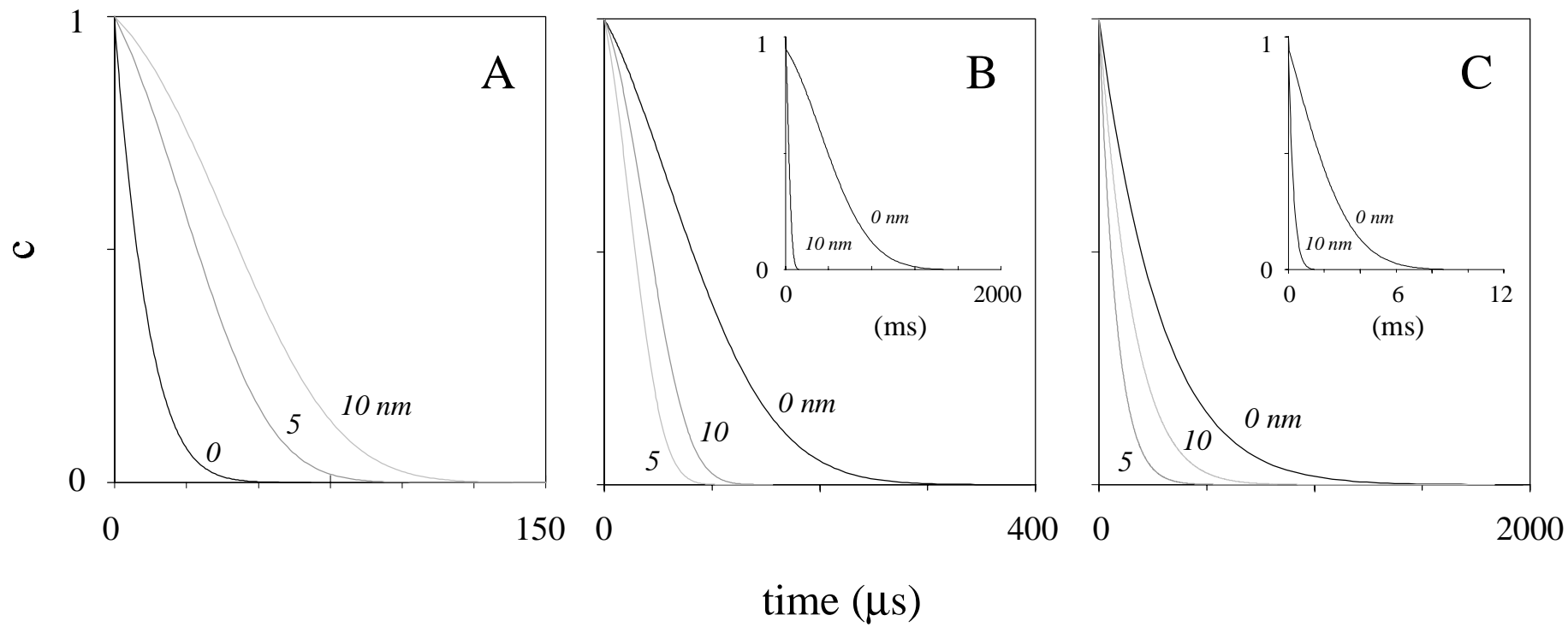
Table 1. Exponent calculated with equation 4.3 and data in Figure 7

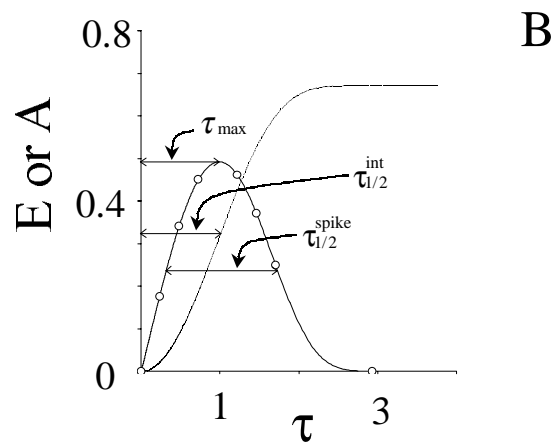
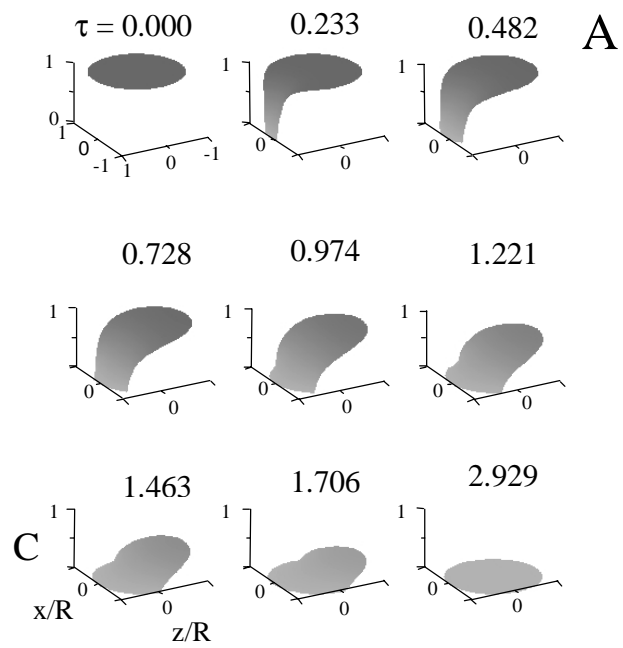
$v \equiv \frac{RV}{2D}$	n [exponent]		
	$t_{1/2}^{\text{int}}$	$t_{1/2}^{\text{spike}}$	t_{max}
P ₁			
< 0.2	1.499	1.499	1.503
0.2-3.4	1.338	1.300	1.412
6.25-25	1.263	1.128	1.124
P ₂			
<0.2	1.499	1.498	1.507
0.2-3.4	1.222		1.001
6.25-25	1.572		0.994

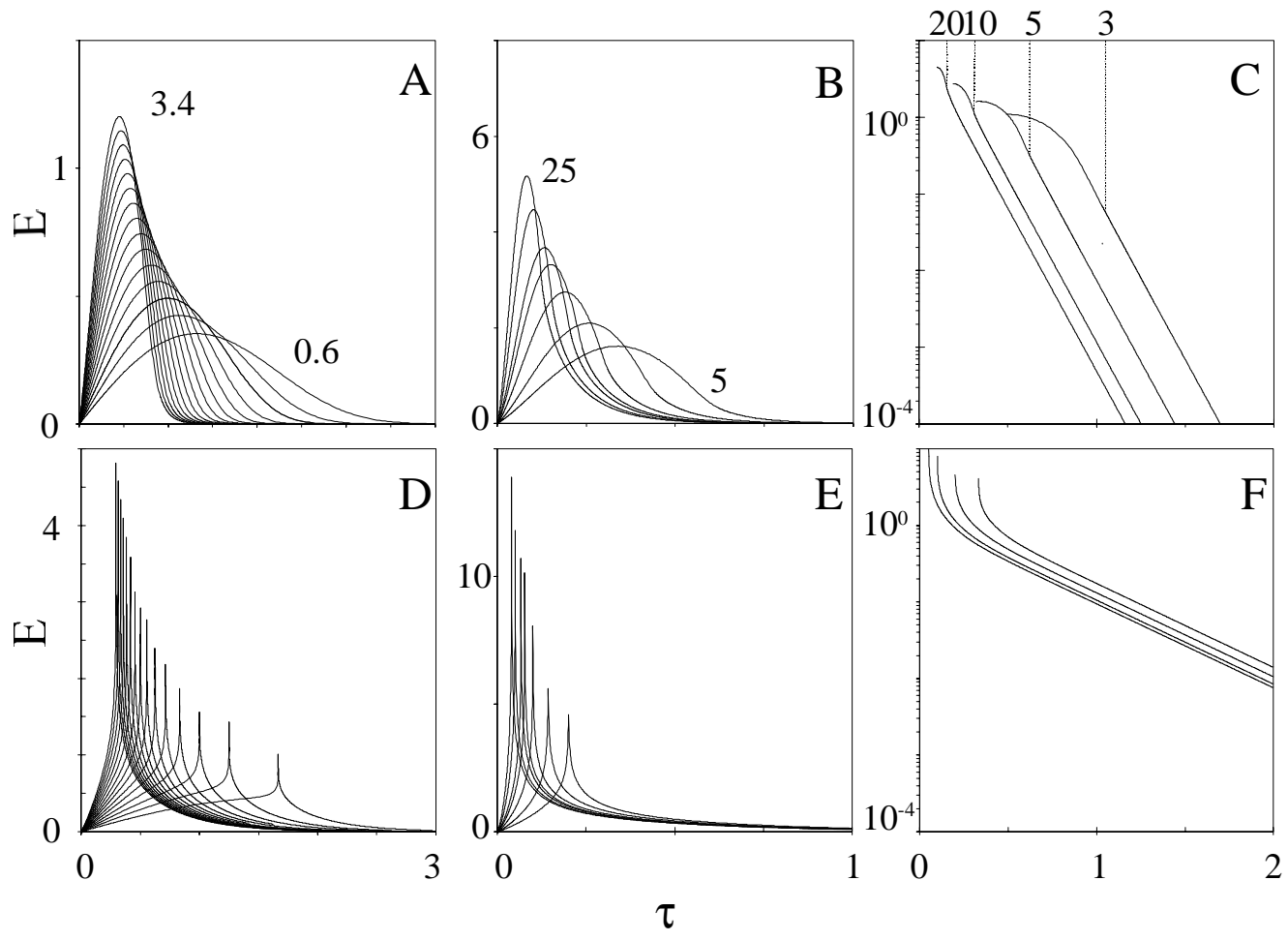


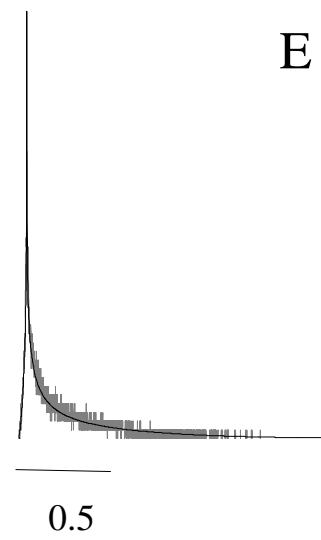
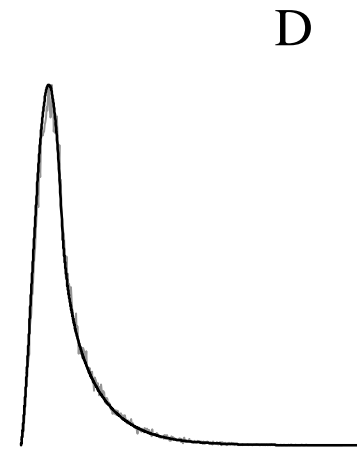
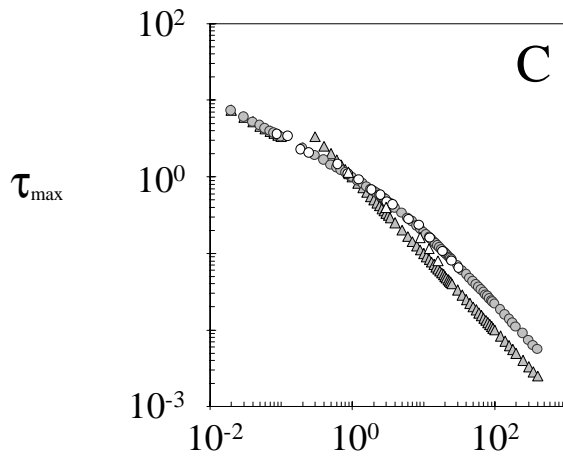
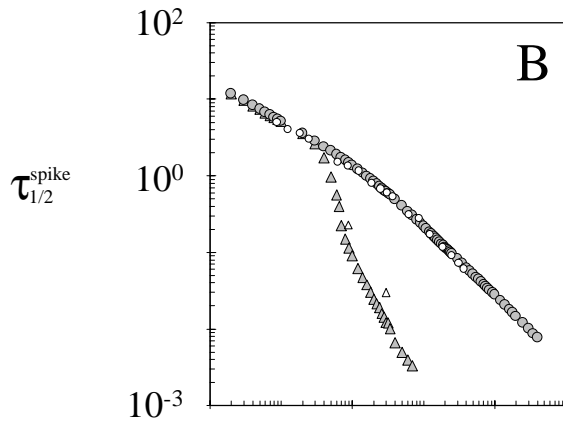
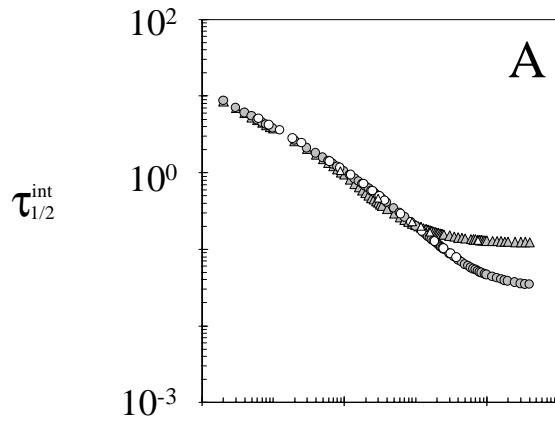


A**B****C**

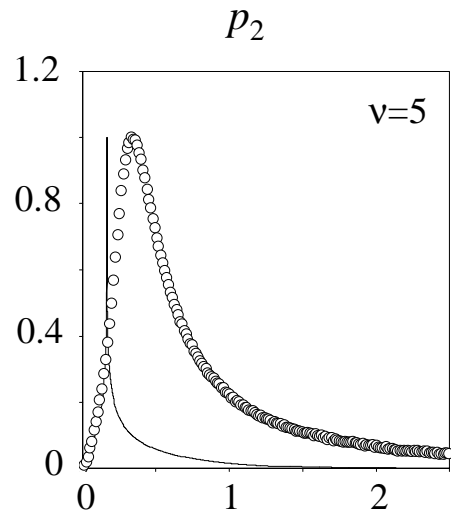
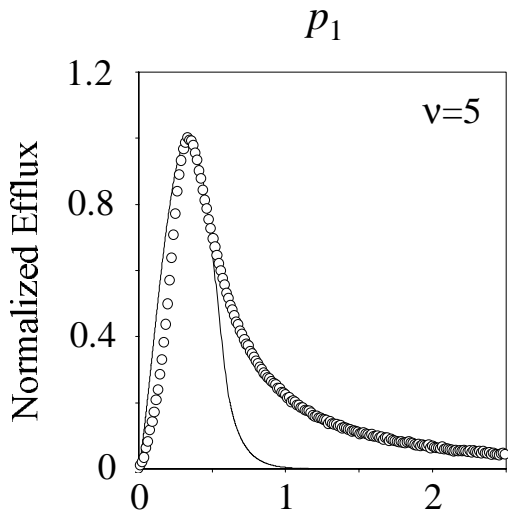




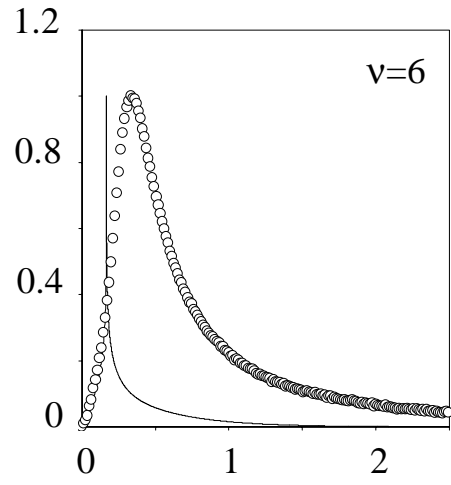
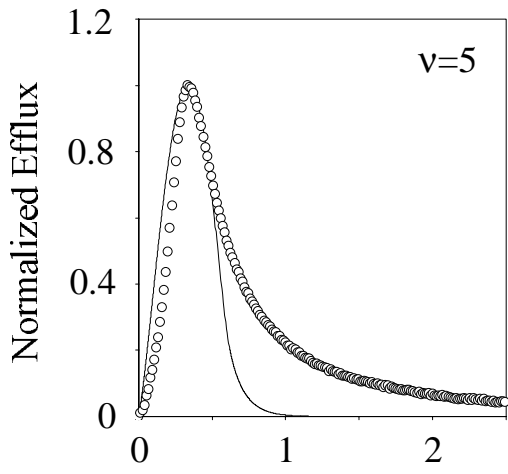




A



B



C

